


Correlated electron–nuclear dynamics of photoinduced water dissociation on rutile TiO₂

Received: 26 February 2023

Accepted: 12 April 2024

Published online: 22 May 2024


 Check for updates

Peiwei You ^{1,2}, Daqiang Chen ^{1,2}, Xinbao Liu^{1,2}, Cui Zhang ^{1,3} , Annabella Selloni ⁴  & Sheng Meng ^{1,2,3} 

Elucidating the mechanism of photoinduced water splitting on TiO₂ is important for advancing the understanding of photocatalysis and the ability to control photocatalytic surface reactions. However, incomplete experimental information and complex coupled electron–nuclear motion make the microscopic understanding challenging. Here we analyse the atomic-scale pathways of photogenerated charge carrier transport and photoinduced water dissociation at the prototypical water–rutile TiO₂(110) interface using first-principles dynamics simulations. Two distinct mechanisms are observed. Field-initiated electron migration leads to adsorbed water dissociation via proton transfer to a surface bridging oxygen. In the other pathway, adsorbed water dissociation occurs via proton donation to a second-layer water molecule coupled to photoexcited-hole transfer promoted by in-plane surface lattice distortions. Two stages of non-adiabatic in-plane lattice motion—expansion and recovery—are observed, which are closely associated with population changes in Ti3*d* orbitals. Controlling such highly correlated electron–nuclear dynamics may provide opportunities for boosting the performance of photocatalytic materials.

Since its ability to photoelectrochemically decompose water was first reported fifty years ago¹, titanium dioxide (TiO₂) has long inspired extensive research and stimulated numerous applications that exploit its excellent catalytic activity, long lifetime of electron–hole pairs and good stability against photocorrosion^{2–5}. The facts that TiO₂ catalyses the splitting of water into H₂ and O₂ under ultraviolet light and doping strategies can extend its photoactivity to the visible range⁶ make TiO₂ one of the key materials in the development of photoelectrochemical cells for solar energy conversion. Understanding the behaviour of photogenerated carriers and the charge transfer pathways at the TiO₂/water interface is, thus, of great relevance and can help improve the performance of TiO₂ in energy-related and environmental applications.

In particular, numerous studies have focused on the water interface with the prototypical rutile TiO₂(110) surface^{7–10}. For example, scanning tunnelling microscopy measurements on TiO₂(110) have provided atomic-scale images of water dissociation at defects^{11,12} and proton transfer to a surface bridging oxygen during processes involving one or few water molecules^{13–15}. Fourier transform infrared spectroscopy experiments detected the stretching frequencies of Ti–O–Ti and Ti–O–H photo-oxidation intermediates at the TiO₂(110)/water interface, based on which a water nucleophilic attack mechanism for O–O coupling was suggested¹⁶. However, experimental studies can only characterize part of the photocatalytic process, and even the prerequisite reaction of water photodissociation is not fully understood.

¹Beijing National Laboratory for Condensed Matter Physics and Institute of Physics, Chinese Academy of Sciences, Beijing, China. ²School of Physical Sciences, University of Chinese Academy of Sciences, Beijing, China. ³Songshan Lake Materials Laboratory, Dongguan, China. ⁴Department of Chemistry, Princeton University, Princeton, NJ, USA.  e-mail: cui Zhang@iphy.ac.cn; aselloni@princeton.edu; smeng@iphy.ac.cn

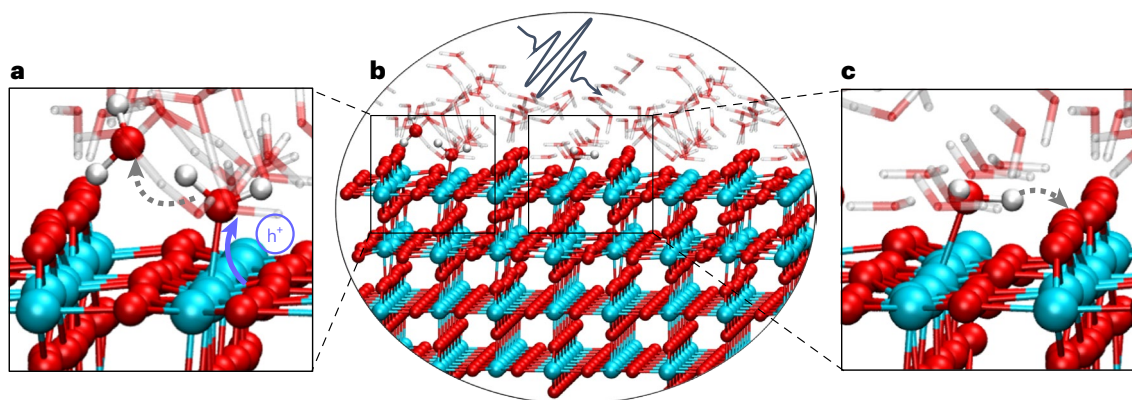


Fig. 1 | Atomic configuration and reaction mechanisms at the TiO₂/water interface. **a**, Schematic of the charge flow in hole-induced splitting dynamics. The blue and dashed arrows indicate the direction of hole current and hole transfer, respectively. **b**, Atomic structure of the TiO₂/water interface, containing

a four-layer TiO₂ slab and 30 water molecules. **c**, Schematic of the field-initiated splitting dynamics. The dashed arrow indicates the direction of proton transfer. The white, red and blue balls denote hydrogen, oxygen and titanium atoms, respectively.

Thus, important challenges remain, most notably characterizing the detailed dynamics of photogenerated electrons and holes at the water/solid interface.

In addition to experimental observations, first-principles calculations have also proven capable to provide atomic-scale insights into water photo-oxidation mechanisms^{17,18}. For example, calculations have revealed that excited carriers in TiO₂ form polarons^{19,20}, which have reduced mobility but still tend to migrate to the surface, thus providing more reaction centres and facilitating photocatalytic reactions^{21–23}. Molecular dynamics (MD) simulations can further reveal energetic and dynamical details of water dissociation^{24,25}, which is the first and, in some cases, the rate-determining step of the oxidation reaction. So far, however, simulations have generally used the adiabatic Born–Oppenheimer approximation on the ground-state potential energy surface without explicitly including the light field and could not provide a complete microscopic picture of how electron–hole pairs were generated and their role in the processes of bond breaking/reforming. These non-adiabatic excited-state processes indeed require a description of excited electronic states and non-adiabatic nuclear motion. The correlated electron–nuclear motion, not included in previous attempts^{26,27}, often leads to phenomena that cannot be described within the Born–Oppenheimer approximation^{28,29}. Moreover, when considering the entangled electron–nuclear dynamics, it is often necessary to model a large number of atoms at a realistic surface or interface, which results in very high computational costs.

Here we investigate the atomistic steps of photoinduced water dissociation at the interface between liquid water and the rutile TiO₂(110) surface using real-time time-dependent density functional theory (rt-TDDFT) MD simulations^{30,31} (Fig. 1a–c). Through first-principles non-adiabatic photoexcitation dynamics, we reveal the microscopic pathways of photogenerated carriers and how the entangled electron–nuclear motion plays a key role in water dissociation. We find that the interplay between electrons and nuclei leads to two distinct water dissociation pathways. Hydrogen bonding of water with surface oxygen atoms introduces a propensity for a field-initiated proton transfer (Fig. 1c). Alternatively, photohole transfer can occur when the adsorbed water is hydrogen bonded to a second-layer water molecule (Fig. 1a). This process is boosted by the formation of a localized exciton on a surface five-coordinated Ti (Ti_{5c}) ion and its four nearest oxygen neighbours (electron–hole polaron or simply polaron hereafter)^{19,32}. The atomic motion with excited phonon modes, correlated with the population change in the photoexcited Ti3d orbitals, can directly drive hole transfer to adsorbed water, accompanied by proton transfer from the latter to the hydrogen-bonded water molecule in the second layer.

Our finding that dynamic polarons participate in hole-driven water dissociation emphasizes the importance of correlated electron–nuclear motion in photocatalysis, a feature that could play a significant role in the photocatalytic properties of other materials, such as perovskites, too.

Field-initiated water dissociation

Although it is well established that water dissociates at the oxygen vacancies of reduced rutile TiO₂(110) (ref. 11), water dissociation on the defect-free rutile surface has been fairly controversial^{33,34}. In our simulations, no water dissociation is observed on a four-layer defect-free rutile slab model during a 2 ps constant-temperature Born–Oppenheimer MD simulation, in agreement with previous studies^{25,34}. However, statistical analysis shows that some OH bonds of the water molecules adsorbed at the Ti_{5c} sites are elongated due to the interaction of their hydrogen atoms either with the adjacent two-fold coordinated bridging oxygen or with the oxygen atoms of nearby water molecules (Supplementary Fig. 1).

We probed the photoexcited dynamics using rt-TDDFT MD to reveal the entangled photocarrier and bond evolution dynamics. A laser pulse with photon energy $E_{\text{photon}} = 3.1$ eV was applied to the TiO₂/water interface, using the velocity-gauge electric field to properly deal with periodic boundary conditions (Methods and Supplementary Note 1). Since one photon can excite only one electron–hole pair in this regime, the light field can be considered as a collection of photons acting over a short period of time. Several independent trajectories were simulated to confirm the main findings, and tests with photon energies of 1.6 and 2.3 eV were performed (Supplementary Fig. 2). In addition, the effects of on-site Hubbard U repulsion on Ti3d electrons (Perdew–Burke–Ernzerhof (PBE)+ U) were examined. As shown in Fig. 2a,b, photoexcited electrons migrated from oxygen to titanium atoms when the light field was turned on. After laser illumination ended at 20 fs, photogenerated electrons were mainly located at the five- and six-fold coordinated titanium atoms (Ti_{5c} and Ti_{6c}, respectively), whereas photogenerated holes were located on the two- and three-fold coordinated oxygen atoms (O_{br} and O_{3c}, respectively) of the TiO₂ surface.

The dissociation dynamics of an adsorbed water molecule forming a hydrogen bond with an adjacent O_{br} site is displayed in Fig. 2c–e. The water molecule dissociates by transferring one proton to the O_{br} atom; therefore, two hydroxyl groups are produced: a terminal hydroxyl on Ti_{5c} and a bridging hydroxyl, O_{br}H, both of which remained stable for the rest of our simulations. The bond breaking and reforming are reflected in the time evolution of bond lengths (Fig. 2c). Similar bond-breaking/bond-reforming mechanisms were reported in recent scanning tunnelling microscopy¹⁵ and molecular-beam³⁵ experiments, although with different estimated reaction energy barriers of 70–120 and 360 meV,

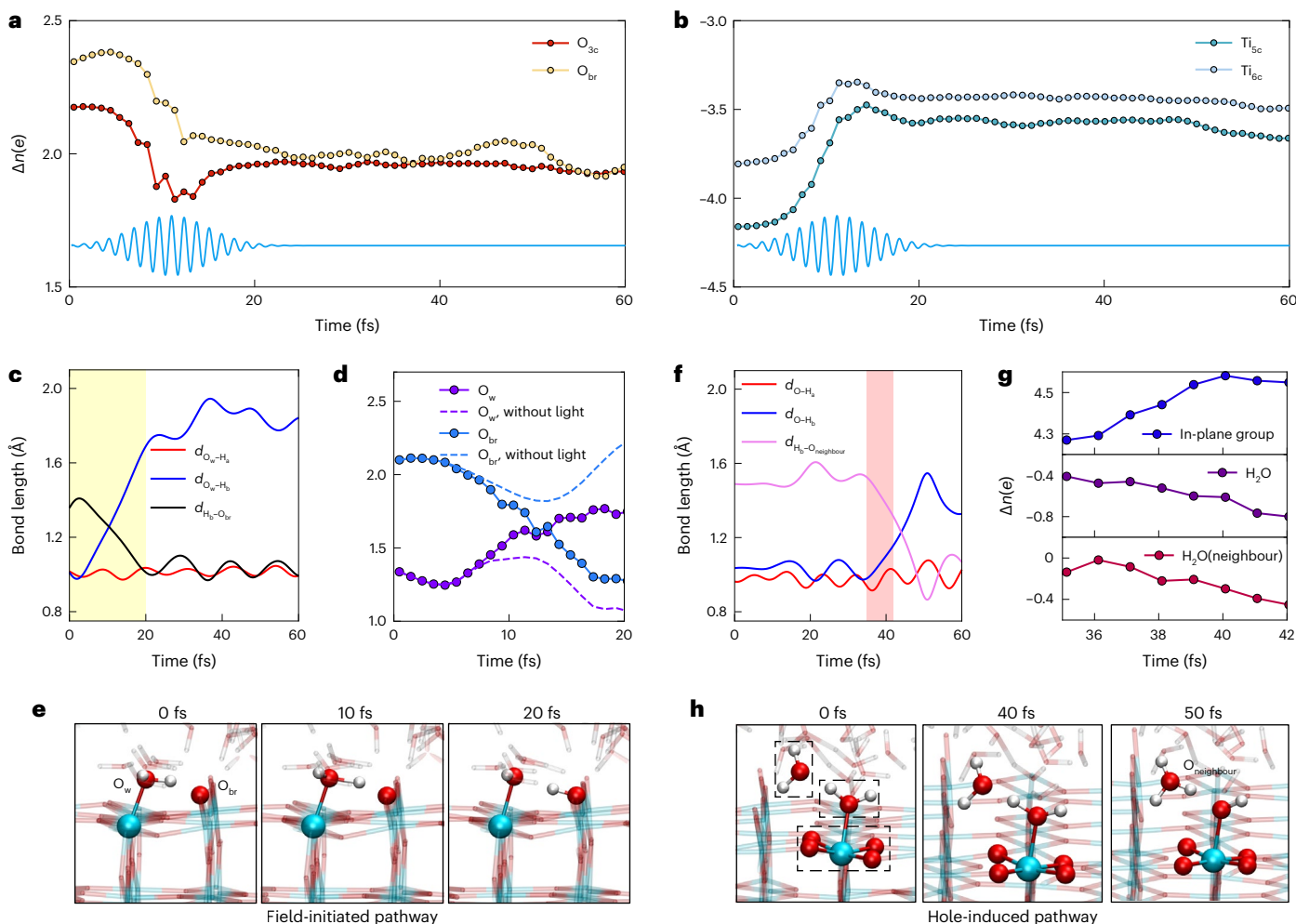


Fig. 2 | Photoinduced water dissociation processes. a, b, Time evolution of Hirshfeld electrons for surface three-coordinated (O_{3c}) and two-coordinated (O_{br}) oxygen atoms (**a**) and surface five-coordinated (Ti_{5c}) and six-coordinated (Ti_{6c}) titanium atoms (**b**) in the presence of a laser pulse. The curve at the bottom of these panels is the envelope of the electric field in the pulse. **c–e**, Field-initiated pathway (left). **c**, Time evolution of adsorbed H_2O bond lengths ($d_{O_w-H_a}$, $d_{O_w-H_b}$) and $O_{br}-H_b$ distance, with the electron transfer reaction time of 20 fs highlighted in yellow. **d**, Time evolution of Hirshfeld electrons of water oxygen (O_w) and O_{br} during the electron redistribution process. **e**, Atomic configurations at 0, 10 and

20 fs, showing that the adsorbed water molecule initially forms a hydrogen bond with an adjacent O_{br} . **f–h**, Hole-induced pathway (right). **f**, Time evolution of H_2O bond lengths and hydrogen-bonded $O_{neighbour}-H_b$ distance, with the hole transfer period of -35–42 fs highlighted in red. **g**, Time evolution of Hirshfeld electrons of in-plane group, H_2O and $H_2O(neighbour)$ between -35 and -42 fs. **h**, Atomic configurations along the hole-driven pathway at 0, 40 and 50 fs, showing that the adsorbed water molecule is hydrogen bonded with a neighbouring H_2O in the second layer before dissociating. The in-plane group is composed of one Ti_{5c} and four neighbouring O_{3c} oxygen atoms.

respectively, possibly due to a field-induced lowering of the barrier in the former experiment¹⁵. In our simulations, bond breaking is associated with a field-promoted electron transfer process from O_{br} to the water oxygen (O_w) in the initial -0–15 fs during laser irradiation, whereas no electron redistribution takes place in the absence of the field (Fig. 2d). Such a field-initiated process is observed with both PBE and PBE+ U functionals. We find that in the initial state, the undercoordinated O_{br} is more electron rich than O_w . This results in an attraction of the proton to O_{br} that promotes electron tunnelling from O_{br} to O_w and thus a weakening of the O_w-H bond, which initiates water dissociation. The increase in the time-dependent projected density of states (PDOS) of O_w along with the concomitant decrease in the PDOS of O_{br} below the Fermi level (Supplementary Fig. 2b) also supports the occurrence of an electron redistribution between O_{br} and O_w . Our simulations show that such a reaction can be triggered if the light-pulse intensity is strong enough, independent of the photon energy (for example, $E_{photon} = 1.6, 2.3$ and 3.1 eV; Supplementary Fig. 2c). The underlying mechanism is, thus, identified as a field-assisted proton transfer from the adsorbed water at Ti_{5c} to O_{br} , where the energy barrier for proton

transfer is lowered by the field and can be easily overcome by thermal fluctuations at $T > 100$ K (ref. 15).

Photohole-driven water dissociation

In addition to the field-initiated water dissociation mechanism described above, our simulations reveal a photohole-driven water decomposition process upon light irradiation where it is the hydrogen bond between adsorbed water and a second-layer water molecule that provides a low barrier for water dissociation. Figure 2f–h shows a H_2O molecule initially adsorbed at a Ti_{5c} site and hydrogen bonded to a neighbouring second-layer H_2O . After -40 fs, the molecule undergoes a splitting reaction (Fig. 2f), producing an OH radical adsorbed on a Ti_{5c} site and hydronium (H_3O^+) in water. This proton-coupled electron transfer process was only observed with $E_{photon} = 3.1$ eV as the water molecule did not dissociate with $E_{photon} = 1.6$ and 2.3 eV, and essentially corresponds to the first step of water photo-oxidation^{17,18,22,36}.

To characterize the transfer process, we investigated the time evolution of the electron population in the adsorbed H_2O , the hydrogen-bonded second-layer $H_2O(neighbour)$ and the in-plane

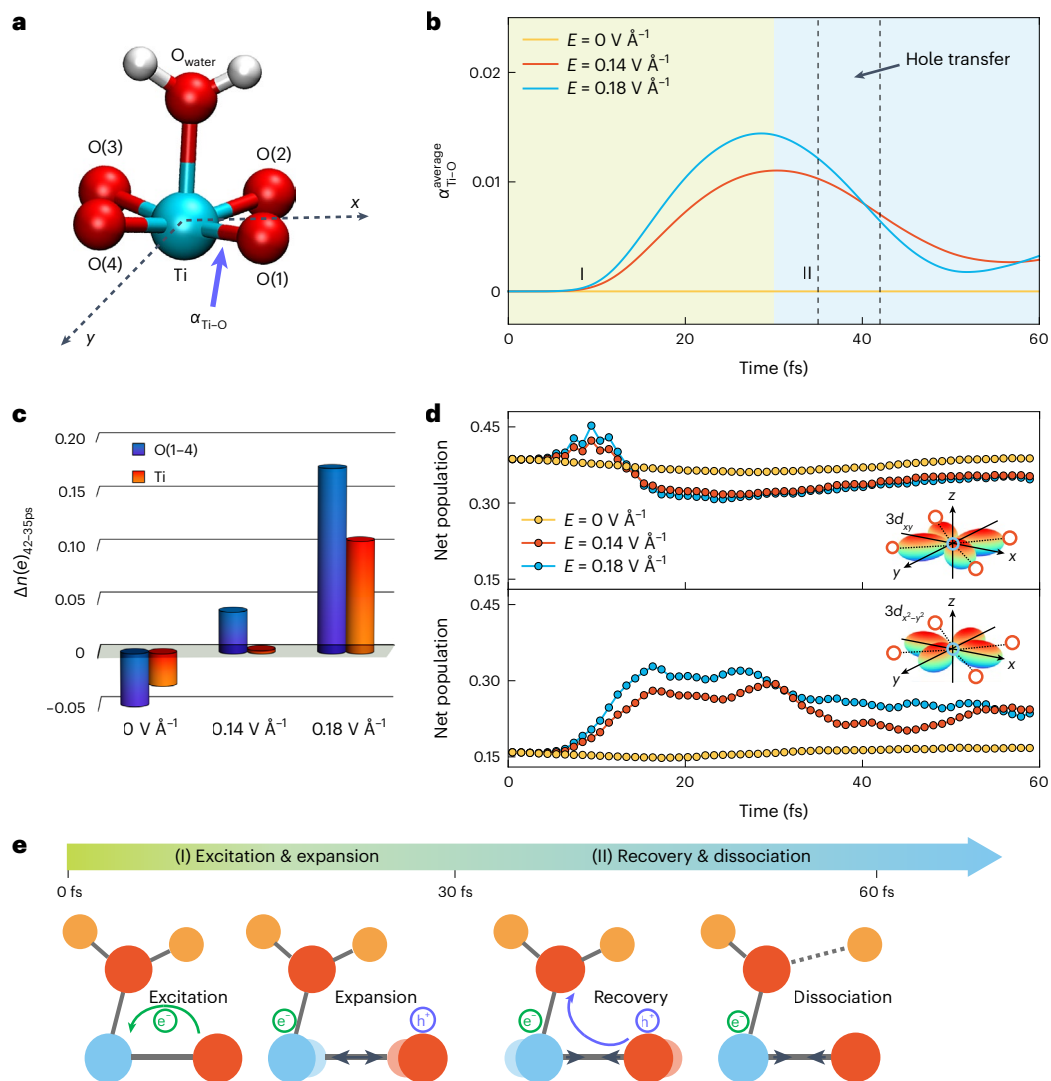


Fig. 3 | Photoexcited-polaron-assisted dynamics. **a**, Atomic structure of the adsorbed H₂O and the Ti and O atoms of the in-plane group, extracted from our simulation of the hole transfer process. The oxygen atoms of water and the in-plane group are labelled as O_{water} and O(1), O(2), O(3) and O(4), respectively. **b**, Time evolution of the photoinduced expansion coefficient averaged over the four Ti–O bonds of the in-plane group. **c**, Difference in the Hirshfeld electron

number from 35 to 42 fs for O(1–4) and Ti under light fields of different intensities. **d**, Net population of Ti $3d_{xy}$ (top) and $3d_{x^2-y^2}$ (bottom) orbitals as a function of time, obtained from the Mulliken charge analysis. **e**, Schematic of the charge flow and water dissociation mechanism assisted by the photoinduced polaron.

photoexcited electron–hole polaron (Fig. 2g). The latter, representing the field-induced charge redistribution (electron–hole pair) with its accompanying lattice distortion³², is localized on the surface Ti_{sc} and its four nearest oxygen atoms (Fig. 2h). Based on the time evolution of the oxygen–hydrogen bond distances (Fig. 2f) and the charge distribution at the reaction site, most of the hole transfer occurs during the time interval of ~35–42 fs, when the water molecule is stretched but still undissociated, before dissociating in the time interval of ~45–50 fs. The decrease in electrons in the adsorbed H₂O and its neighbouring H₂O indicates hole transfer from TiO₂, which is mainly contributed by the in-plane group (Fig. 2g; also confirmed by the Bader charge analysis shown in Supplementary Fig. 3). This hole transfer process results in a weakening of the interaction between hydrogen and oxygen atoms in the adsorbed H₂O, leading to the subsequent deprotonation reaction. A comparison of the reactive trajectories (where water dissociation occurred) with non-reactive ones (without dissociation) highlights the important role of hydrogen bonding and hole transfer (Supplementary Fig. 4). Our results suggest an apparent quantum efficiency of 1% (Supplementary Note 5).

This is higher than the value of 0.25% found experimentally¹³, which may in part be attributed to the higher water coverage in our simulations. Complementing existing experimental and computational studies of the intermediates and barriers of water photo-oxidation on TiO₂(110) (refs. 16,22,36), these non-adiabatic dynamics simulations, thus, reveal the key role of surface electron–hole polarons in the hole-driven water dissociation.

Correlated electron–nuclear dynamics

To characterize the correlated electron–nuclear dynamics of the dissociating H₂O and the in-plane group during the hole transfer process, we define the photoinduced expansion coefficient of a Ti–O bond as $\alpha_{\text{Ti-O}} = [d_E(t) - d_0(t)]/d_0(t)$, where $d_E(t)$ is the Ti–O bond distance under a light field strength of E . We average $\alpha_{\text{Ti-O}}$ over the four Ti–O bonds of the in-plane group (Fig. 3a) and compare the $\alpha_{\text{Ti-O}}^{\text{average}}$ value obtained at $E = 0.14$ and 0.18 V \AA^{-1} with the case without photoexcitation ($E = 0 \text{ V \AA}^{-1}$) (Fig. 3b). During the period of ~0–30 fs, the average photoinduced expansion coefficient $\alpha_{\text{Ti-O}}^{\text{average}}$ is positive and increasing relative to the case without light, indicating that the Ti–O lattice

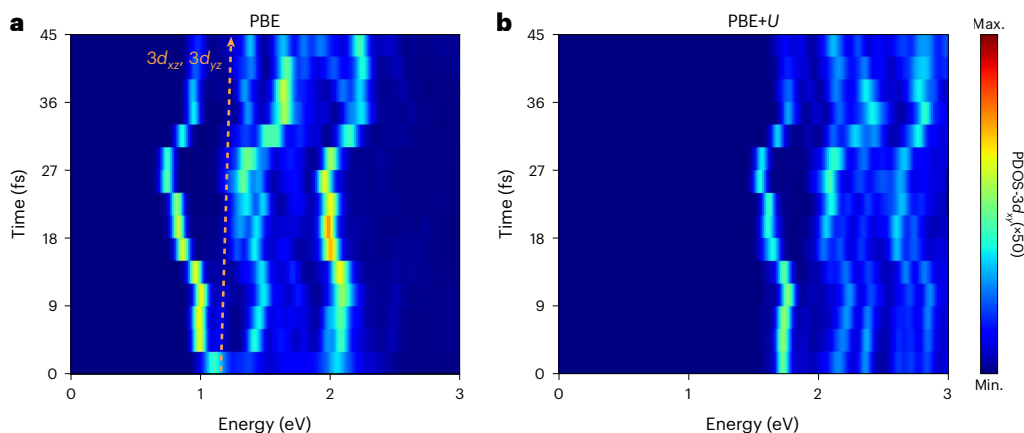


Fig. 4 | Photoinduced shift of the 3d electron energy level in the TiO₂ surface polaron. a, b, Time evolution of the PDOS of the Ti3d_{xy} orbital computed using the PBE (a) and PBE+U (b) functionals. The energy zero is set at the Fermi

level, in the middle of the TiO₂ bandgap. The field strength of the laser pulse is $E = 0.18 \text{ V \AA}^{-1}$. The orange dashed line schematically indicates the slight shift of the Ti3d_{xz} and Ti3d_{yz} orbitals during the time evolution.

distortion undergoes in-plane expansion during irradiation (charge transfers are shown in Supplementary Fig. 5).

For the photoexcited electron, we consider the population of localized 3d orbitals on the Ti atom. We divide the Mulliken charge populations of 3d electrons into two parts: the net population localized on a certain orbital and the population overlapping with other orbitals (Methods and Supplementary Note 4). Figure 3d compares the net population of the 3d_{xy} and 3d_{x²-y²} orbitals (which contribute the most; Supplementary Fig. 6) under field strengths of $E = 0.14$ and 0.18 V \AA^{-1} with respect to the light-free case. In the first 15 fs of electronic excitation, the increase in photoexcited net populations of 3d_{xy} and 3d_{x²-y²} leads to repulsive forces along the Ti–O bonds (Supplementary Fig. 7), resulting in a continuous expansion of the in-plane group until 30 fs.

In the subsequent period of ~30–60 fs, the decrease in $\alpha_{\text{Ti-O}}^{\text{average}}$ indicates the recovery of the Ti–O lattice distortion after photoexcitation, accompanied by hole transfer during ~35–42 fs. Owing to the relaxation and charge population redistribution in the Ti3d orbitals, the repulsion forces along the Ti–O bonds decrease after 15 fs, so that at about 30 fs, the lattice expansion starts to decline. This process changes the electrostatic potential, inducing electrons to flow from the adsorbed water to the surface Ti–O bonds. At a field strength of 0.18 V \AA^{-1} , Hirshfeld electrons on the oxygens and titanium of the in-plane group increase significantly during the period of ~35–42 fs (Fig. 3c), indicating hole transfer from the in-plane group to the adsorbed water molecule through the titanium atom. The photogenerated electron stays on Ti_{sc} in our simulation; it may actually relax via long-term non-thermal/thermal effects or contribute to hydrogen production in the physical system. Further reaction steps are required to complete the production of H₂ and O₂ (Supplementary Fig. 8). The water molecule dissociates when the field strength is large enough to trigger the hole transfer, and water adsorption is enhanced (Supplementary Figs. 9 and 10).

Altogether, our results suggest a two-stage polaron-assisted mechanism for photohole-driven water dissociation: (I) excitation and expansion followed by (II) recovery and dissociation (Fig. 3e). In the first stage (~0–30 fs), photoexcited electron transfer takes place from the oxygens to the titanium atom in the in-plane group, inducing a dynamic expansion of the lattice. In the second stage (~30–60 fs), the recovery process occurs. This is ascribed to the redistribution/relaxation of the localized 3d electrons at the titanium site, which promotes the flow of electrons from the water molecule to the TiO₂ surface. In Supplementary Fig. 11, the PDOS of the water molecule and in-plane group shifts towards the energy levels of photoholes. This shift and broadening of the bands of adsorbed water suggest the opening

of a hole transfer channel. In addition, the dominant photoexcited phonon modes in this process are calculated (Supplementary Note 6 and Supplementary Fig. 12). The projected phonon intensities exhibit changes in the presence of the light field, indicating that the E_u and A_{1g} modes are excited. Such analysis, thus, confirms that the photoinduced expansion–recovery changes characterize the coupling between photoexcited phonons and photogenerated electron–hole pairs.

The expansion and recovery mechanism discussed above can also be considered as a ‘real-time’ dynamic Jahn–Teller distortion^{37,38} in the photoexcited state. The fingerprint of such a process is the energy-level splitting or lowering of the 3d_{xy} electrons, whereas the 3d_{yz} or 3d_{xz} orbitals are slightly shifted up. Figure 4 shows the time evolution of the PDOS for the Ti3d_{xy} orbital. The results obtained with both PBE functional and Hubbard on-site energy correction show the typical energy-level shift in the dynamic Jahn–Teller distortion. With a light intensity of 0.18 V \AA^{-1} , the energy edge of the Ti3d_{xy} PDOS moves from an initial 1.1 to 0.7 eV at 27 fs and then returns to 1.1 eV, corresponding to the expansion–recovery process of the photoinduced lattice distortion. A similar behaviour of the PDOS energy edge is observed with the PBE+U approach (Fig. 4b). In contrast, the PDOS energy edge exhibits only weak oscillations at ~1 eV in the absence of illumination (Supplementary Fig. 13). Such an energy-level shift in the 3d_{xy} orbital can be considered as the excited-state analogue of the defect state of excess electrons in reduced TiO₂ (refs. 21,39).

Experimental validation of the mechanisms of hole-driven water dissociation and correlated electron–nuclear dynamics found in our simulations may be provided by measurements similar to those employed for the detection of excited defect states in reduced TiO₂ (ref. 40). Specifically, time-resolved absorption spectroscopy and two-photon photoemission spectroscopy could measure the enhancement and attenuation of photoabsorption (Supplementary Fig. 14) to confirm the proposed polaron-assisted mechanism^{41–43}. Furthermore, with the development of attosecond science, ultrafast electron diffraction and/or X-ray spectroscopy^{41,44} experiments (with a time resolution of <1 fs) are expected to enable the measurements of lattice motion and phonon fingerprints of the polarons (Supplementary Fig. 15). Alternatively, the excited phonon modes at the aqueous oxide interface may be measured using Raman spectroscopy under ultraviolet irradiation to detect the polaron-assisted mechanism. Charge carrier dynamics and vibrational modes of product species could also be measured by appropriate experimental techniques (Supplementary Figs. 16 and 17).

In conclusion, non-adiabatic quantum dynamics simulations based on rt-TDDFT provide a direct view of how the photogenerated charge carriers couple with nuclear motion during water photodissociation

at the water/TiO₂ interface. Water dissociation promoted by hydrogen bonding to a surface bridging oxygen is a field-initiated process that may be expected to occur on several metal oxide surfaces. The photoexcited-hole-transfer-driven mechanism shows that the water dissociation is strongly coupled with the dynamic lattice distortion (photoexcited phonons) on the TiO₂ surface. The formation and expansion of the in-plane group are dominated by the carrier flow in the Ti3d orbitals. In the recovery phase of the polaron, the contraction of titanium–oxygen bonds promotes hole transfer from TiO₂ to water, leading to water decomposition. Analysis of several independent non-adiabatic trajectories shows that the ratio of hole-induced and field-initiated water dissociation is -1.25, suggesting that these two processes make similarly important contributions to water photodissociation reactions at the interface. These results pave the way to a comprehensive understanding of photoinduced water dissociation on TiO₂, revealing a polaron-assisted hole transfer mechanism that could be applied to interpret and control a wide range of photocatalytic reactions.

Online content

Any methods, additional references, Nature Portfolio reporting summaries, source data, extended data, supplementary information, acknowledgements, peer review information; details of author contributions and competing interests; and statements of data and code availability are available at <https://doi.org/10.1038/s41563-024-01900-5>.

References

1. Fujishima, A. & Honda, K. Electrochemical photolysis of water at a semiconductor electrode. *Nature* **238**, 37–38 (1972).
2. Khan, S. U. M., Al-Shahry, M. & Ingler, W. B. Efficient photochemical water splitting by a chemically modified n-TiO₂. *Science* **297**, 2243–2245 (2002).
3. Hashimoto, K., Irie, H. & Fujishima, A. TiO₂ photocatalysis: a historical overview and future prospects. *Jpn. J. Appl. Phys.* **44**, 8269–8285 (2005).
4. Schneider, J. et al. Understanding TiO₂ photocatalysis: mechanisms and materials. *Chem. Rev.* **114**, 9919–9986 (2014).
5. Guo Q., Zhou C., Ma Z. & Yang X. Fundamentals of TiO₂ photocatalysis: concepts, mechanisms, and challenges. *Adv. Mater.* **31**, 1901997 (2019).
6. Anpo, M. & Takeuchi, M. The design and development of highly reactive titanium oxide photocatalysts operating under visible light irradiation. *J. Catal.* **216**, 505–516 (2003).
7. Yin, W.-J., Wen, B., Zhou, C., Selloni, A. & Liu, L.-M. Excess electrons in reduced rutile and anatase TiO₂. *Surf. Sci. Rep.* **73**, 58–82 (2018).
8. Ma, Y. et al. Titanium dioxide-based nanomaterials for photocatalytic fuel generations. *Chem. Rev.* **114**, 9987–10043 (2014).
9. Bourikas, K., Kordulis, C. & Lycourghiotis, A. Titanium dioxide (anatase and rutile): surface chemistry, liquid-solid interface chemistry, and scientific synthesis of supported catalysts. *Chem. Rev.* **114**, 9754–9823 (2014).
10. Kowalski, P. M., Camellone, M. F., Nair, N. N., Meyer, B. & Marx, D. Charge localization dynamics induced by oxygen vacancies on the TiO₂(110) surface. *Phys. Rev. Lett.* **105**, 146405 (2010).
11. Bikondoa, O. et al. Direct visualization of defect-mediated dissociation of water on TiO₂(110). *Nat. Mater.* **5**, 189–192 (2006).
12. Wendt, S. et al. Formation and splitting of paired hydroxyl groups on reduced TiO₂(110). *Phys. Rev. Lett.* **96**, 066107 (2006).
13. Tan, S. et al. Observation of photocatalytic dissociation of water on terminal Ti sites of TiO₂(110)-1×1 surface. *J. Am. Chem. Soc.* **134**, 9978–9985 (2012).
14. Yang, W. et al. Effect of the hydrogen bond in photoinduced water dissociation: a double-edged sword. *J. Phys. Chem. Lett.* **7**, 603–608 (2016).
15. Tan, S. et al. Interfacial hydrogen-bonding dynamics in surface-facilitated dehydrogenation of water on TiO₂(110). *J. Am. Chem. Soc.* **142**, 826–834 (2020).
16. Nakamura, R. & Nakato, Y. Primary intermediates of oxygen photoevolution reaction on TiO₂ (rutile) particles, revealed by in situ FTIR absorption and photoluminescence measurements. *J. Am. Chem. Soc.* **126**, 1290–1298 (2004).
17. Wang, D., Sheng, T., Chen, J., Wang, H.-F. & Hu, P. Identifying the key obstacle in photocatalytic oxygen evolution on rutile TiO₂. *Nat. Catal.* **1**, 291–299 (2018).
18. Migani, A. & Blancafort, L. What controls photocatalytic water oxidation on rutile TiO₂(110) under ultra-high-vacuum conditions? *J. Am. Chem. Soc.* **139**, 11845–11856 (2017).
19. Franchini, C., Reticcioli, M., Setvin, M. & Diebold, U. Polarons in materials. *Nat. Rev. Mater.* **6**, 560–586 (2021).
20. Rousseau, R., Glezakou, V.-A. & Selloni, A. Theoretical insights into the surface physics and chemistry of redox-active oxides. *Nat. Rev. Mater.* **5**, 460–475 (2020).
21. Di Valentin, C. & Selloni, A. Bulk and surface polarons in photoexcited anatase TiO₂. *J. Phys. Chem. Lett.* **2**, 2223–2228 (2011).
22. Cheng, J., VandeVondele, J. & Sprik, M. Identifying trapped electronic holes at the aqueous TiO₂ interface. *J. Phys. Chem. C* **118**, 5437–5444 (2014).
23. Selcuk, S. & Selloni, A. Facet-dependent trapping and dynamics of excess electrons at anatase TiO₂ surfaces and aqueous interfaces. *Nat. Mater.* **15**, 1107–1112 (2016).
24. Cheng, J. & Sprik, M. Acidity of the aqueous rutile TiO₂(110) surface from density functional theory based molecular dynamics. *J. Chem. Theory Comput.* **6**, 880–889 (2010).
25. Liu, L.-M., Zhang, C., Thornton, G. & Michaelides, A. Structure and dynamics of liquid water on rutile TiO₂(110). *Phys. Rev. B* **82**, 161415 (2010).
26. Long, R., Fang, W.-H. & Prezhdo, O. V. Strong interaction at the perovskite/TiO₂ interface facilitates ultrafast photoinduced charge separation: a nonadiabatic molecular dynamics study. *J. Phys. Chem. C* **121**, 3797–3806 (2017).
27. Cheng, C., Fang, W. H., Long, R. & Prezhdo, O. V. Water splitting with a single-atom Cu/TiO₂ photocatalyst: atomistic origin of high efficiency and proposed enhancement by spin selection. *JACS Au* **1**, 550–559 (2021).
28. Pisana, S. et al. Breakdown of the adiabatic Born-Oppenheimer approximation in graphene. *Nat. Mater.* **6**, 198–201 (2007).
29. Che, L. et al. Breakdown of the Born-Oppenheimer approximation in the F + o-D₂ → DF + D reaction. *Science* **317**, 1061–1064 (2007).
30. Lian, C., Guan, M., Hu, S., Zhang, J. & Meng, S. Photoexcitation in solids: first-principles quantum simulations by real-time TDDFT. *Adv. Theory Simul.* **1**, 1800055 (2018).
31. You P., Chen D., Lian C., Zhang C. & Meng S. First-principles dynamics of photoexcited molecules and materials towards a quantum description. *WIREs Comput. Mol. Sci.* **11**, e1492 (2020).
32. Carneiro, L. M. et al. Excitation-wavelength-dependent small polaron trapping of photoexcited carriers in α-Fe₂O₃. *Nat. Mater.* **16**, 819–825 (2017).
33. Diebold, U. Perspective: a controversial benchmark system for water-oxide interfaces: H₂O/TiO₂(110). *J. Chem. Phys.* **147**, 040901 (2017).
34. Wen, B., Calegari Andrade, M. F., Liu, L. M. & Selloni, A. Water dissociation at the water-rutile TiO₂(110) interface from ab initio-based deep neural network simulations. *Proc. Natl Acad. Sci. USA* **120**, e2212250120 (2023).
35. Wang, Z. T. et al. Probing equilibrium of molecular and deprotonated water on TiO₂(110). *Proc. Natl Acad. Sci. USA* **114**, 1801–1805 (2017).
36. Li, Y.-F. & Selloni, A. Pathway of photocatalytic oxygen evolution on aqueous TiO₂ anatase and insights into the different activities of anatase and rutile. *ACS Catal.* **6**, 4769–4774 (2016).

37. Burns, P. C. & Hawthorne, F. C. Static and dynamic Jahn-Teller effects in Cu^{2+} oxysalt minerals. *Can. Mineral.* **34**, 1089–1105 (1996).
38. Fu, K. M. et al. Observation of the dynamic Jahn-Teller effect in the excited states of nitrogen-vacancy centers in diamond. *Phys. Rev. Lett.* **103**, 256404 (2009).
39. Di Valentin, C., Pacchioni, G. & Selloni, A. Electronic structure of defect states in hydroxylated and reduced rutile $\text{TiO}_2(110)$ surfaces. *Phys. Rev. Lett.* **97**, 166803 (2006).
40. Wang, Z. et al. Localized excitation of Ti^{3+} ions in the photoabsorption and photocatalytic activity of reduced rutile TiO_2 . *J. Am. Chem. Soc.* **137**, 9146–9152 (2015).
41. Sidiropoulos, T. P. H. et al. Probing the energy conversion pathways between light, carriers, and lattice in real time with attosecond core-level spectroscopy. *Phys. Rev. X* **11**, 041060 (2021).
42. Wagstaffe, M. et al. Photoinduced dynamics at the water/ $\text{TiO}_2(101)$ interface. *Phys. Rev. Lett.* **130**, 108001 (2023).
43. Chen, X. et al. The formation time of $\text{Ti-O}\cdot$ and $\text{Ti-O}\cdot\text{-Ti}$ radicals at the n-Sr TiO_3 /aqueous interface during photocatalytic water oxidation. *J. Am. Chem. Soc.* **139**, 1830–1841 (2017).
44. Kim, H. Y. et al. Attosecond field emission. *Nature* **613**, 662–666 (2023).

Publisher's note Springer Nature remains neutral with regard to jurisdictional claims in published maps and institutional affiliations.

Springer Nature or its licensor (e.g. a society or other partner) holds exclusive rights to this article under a publishing agreement with the author(s) or other rightsholder(s); author self-archiving of the accepted manuscript version of this article is solely governed by the terms of such publishing agreement and applicable law.

© The Author(s), under exclusive licence to Springer Nature Limited 2024

Methods

The rt-TDDFT MD simulations were performed using the time-dependent ab initio package^{30,31}. Born–Oppenheimer MD simulations and ground-state calculations were carried out with the SIESTA code⁴⁵. We used a four-layer-thick TiO₂(110) slab with a 2 × 4 surface supercell in contact with a liquid layer of 30 water molecules at a density of -1 g cm⁻². The dimensions of the TiO₂/water interface supercell were 13.14 Å × 11.98 Å × 30.00 Å, with a vacuum space of 13.00 Å above the water layer. Only the Γ point was used for the electron dynamics simulations. We considered a laser field polarized along the *x* direction with a photon energy of 3.1 eV and an intensity of 0.18 V Å⁻¹. The full-width at half-maximum of the light pulse was 8 fs. The injected energy fluence during 20 fs was 3.1 mJ cm⁻², which is much smaller than the total injected energy of 3.6 J cm⁻² during 1 h light irradiation in experiments¹³. Given the ultrafast photon–surface interaction time in our simulations, the light field intensity used provides a reasonable approximation of that in solar irradiation. We employed the generalized gradient approximation of PBE⁴⁶ for the exchange and correlation energy and a numerical atomic orbital basis set with an energy cutoff of 200 Ry for the plane-wave expansion of charge density. We considered the influence of on-site Hubbard *U* repulsion on 3*d* electrons of Ti using the corrected functional scheme of Dudarev (PBE+*U*)⁴⁷ and chose a *U* value of 4.2 eV, as suggested elsewhere¹⁰. The energy gap calculated with the PBE+*U* functional is 0.5 eV larger than that given by PBE, which can be fully covered by the frequency spectrum of the light pulse. The excited-band structure of TiO₂ obtained from the PBE functional and the PBE+*U* method exhibits very similar photoexcitation behaviours and features near the Γ point on irradiation (Supplementary Fig. 18).

We first equilibrated the TiO₂/water interface system within the canonical ensemble (NVT) at 300 K for 2 ps. To capture the quantum dynamics of photocatalytic water splitting in the light field, the time-dependent Kohn–Sham wavefunctions of the interface were evolved for up to 2,000 steps in the microcanonical ensemble (NVE) with a time step of 30 as. The first-order Crank–Nicholson scheme was used for time propagation in the Ehrenfest scheme. We applied the climbing-image nudged elastic band method⁴⁸ as implemented in the Vienna ab initio simulation package⁴⁹ to evaluate the energy barrier of hydrogen diffusion and production on the rutile surface. The force thresholds of the transition state and structure relaxation were set to 0.06 and 0.01 eV Å⁻¹, respectively.

Hirshfeld electron analysis is used to specify the real-space charge distribution in the charge transfer process (Supplementary Note 3). Note that the calculated charge is scaled by a factor 10 to emphasize the changes. Such excited (hot) electrons or holes are effective in changing the potential energy surface and initiate the structural response. Although Mulliken charge assumes ‘half-and-half division’ of the overlap population, Hirshfeld or Bader charge analysis divides the system into well-defined atomic fragments, which concisely describe the molecular charge reorganization. We separate Mulliken charge into two parts: the net population localized on a certain orbital and the population overlapping with other orbitals (Supplementary Note 4). Therefore, we use the net populations in the Mulliken charge analysis to display the time-resolved charge exchange on different orbitals, and Hirshfeld charge analysis to quantitatively reveal the charge transfer process in the reaction.

Data availability

The data that support the findings of this study are available via GitLab at <https://gitlab.com/tddft/water-on-rutile-tio2>.

Code availability

The code that was used to simulate the findings of this study is available from the corresponding authors upon reasonable request.

References

- Garcia, A. et al. SIESTA: recent developments and applications. *J. Chem. Phys.* **152**, 204108 (2020).
- Perdew, J. P., Burke, K. & Ernzerhof, M. Generalized gradient approximation made simple. *Phys. Rev. Lett.* **77**, 3865–3868 (1996).
- Dudarev, S. L., Botton, G. A., Savrasov, S. Y., Humphreys, C. J. & Sutton, A. P. Electron-energy-loss spectra and the structural stability of nickel oxide: an LSDA+*U* study. *Phys. Rev. B* **57**, 1505–1509 (1998).
- Sheppard, D., Xiao, P., Chemelewski, W., Johnson, D. D. & Henkelman, G. A generalized solid-state nudged elastic band method. *J. Chem. Phys.* **136**, 074103 (2012).
- Kresse, G. & Furthmüller, J. Efficiency of ab-initio total energy calculations for metals and semiconductors using a plane-wave basis set. *Comp. Mater. Sci.* **6**, 15–50 (1996).

Acknowledgements

We acknowledge financial support from MOST (grant nos. 2021YFA1400201 and 2021YFA1400503), NSFC (grant nos. 11974400, 12025407, 11934003 and 92250303), CAS Project for Young Scientists in Basic Research YSBR-047 and ‘Strategic Priority Research Program B’ of the CAS (no. XDB330301). A.S. was supported by Department of Energy Basic Energy Sciences, Chemical Sciences, Geosciences, & Biosciences Division, under award DE-SC0007347. P.Y. thanks Y. Wu for encouragement and discussions.

Author contributions

P.Y. and S.M. proposed the project. C.Z., A.S. and S.M. conceived and supervised this project. P.Y. carried out the simulations and performed the analysis. P.Y., X.L. and D.C. developed the methodologies and analysis codes. P.Y., C.Z., A.S. and S.M. interpreted the analysis and wrote the manuscript. All authors contributed to the discussions and revisions of the manuscript.

Competing interests

The authors declare no competing interests.

Additional information

Supplementary information The online version contains supplementary material available at <https://doi.org/10.1038/s41563-024-01900-5>.

Correspondence and requests for materials should be addressed to Cui Zhang, Annabella Selloni or Sheng Meng.

Peer review information *Nature Materials* thanks Tanja Cuk and the other, anonymous, reviewer(s) for their contribution to the peer review of this work.

Reprints and permissions information is available at www.nature.com/reprints.